Appl. Phys. B 70, 689–694 (2000) / Digital Object Identifier (DOI) 10.1007/s003400000266

Applied Physics B
Lasers
and Optics

Nanoscale focusing of atoms with a pulsed standing wave

M. Mützel, D. Haubrich, D. Meschede

Institut für Angewandte Physik, Rheinische Friedrich-Wilhelms-Universität Bonn, Wegelerstr. 8, 53115 Bonn, Germany
(E-mail: sek@iap.uni-bonn.de)

Received: 6 October 1999/Revised version: 3 February 2000/Published online: 5 April 2000 –

Abstract. We have theoretically and experimentally investigated the focusing properties of a detuned pulsed standing wave onto a beam of neutral atoms. In close analogy to the continuous-wave situation the dipole force leads to a periodic focusing of atoms with a period of $\lambda/2$, provided an adiabatic condition is fulfilled. Pulsed laser light is conveniently converted to short wavelengths and hence offers advantages in the application of atom lithography with elements of technological interest having blue or UV resonance lines.

PACS: 03.75.Be; 32.80.Pj; 42.50.Vk

The periodic focusing of atomic beams by means of a standing wave light field is a key experiment in atom lithography and was first demonstrated with sodium in 1992 [1]. In the simplest case a one-dimensional standing wave of near resonant laser light acts as a microlens array which concentrates the flux of an atomic beam into parallel lines spaced by half the wavelength λ of the light field and having widths of only several tens of nanometers [2].

One line of research seeks to extend the method of atom lithography to technologically relevant materials. Many elements of interest, for instance from group III of the periodic table, generally have short-wavelength resonance lines in the blue or UV, requiring a frequency-doubled laser light source. Most experiments so far have been performed with chromium ($\lambda = 426$ nm) [3, 4] where also two-dimensional structures have been produced [5, 6]. Using a $\lambda = 309$ nm standing wave, periodic lines of aluminum have been deposited onto a substrate [7].

Efficient frequency doubling of continuous wave (cw) lasers requires power enhancement cavities and servo loops in order to obtain sufficiently strong conversion. Modelocked pulsed laser sources on the other hand offer a conversion efficiency of 20% or more in a single pass of a suitable nonlinear crystal, i.e. with little effort. We have therefore explored the applicability of a near-resonant pulsed standing wave for focusing of atomic beams at the nanometer scale in an attempt to eliminate complex frequency conversion schemes for atoms with UV resonance lines. For simplicity, however, we have used the fundamental of a mode-locked Ti:sapphire laser (Spectra Physics Tsunami) at 852 nm and a cesium atomic beam apparatus which has been described in detail in [8] for experimental investigations but there is no conceptual difference to the application with other species using frequency-doubled laser light. This work also extends earlier experiments with an on-resonance pulsed standing wave, where we have demonstrated the macroscopic focusing of a slow atomic beam [9].

1 Theoretical description

It is well known [10] that a two-level atom in a continuous standing wave is subject to a dipole force which formally can be derived from a potential

$$U_{\mathrm{cw}}(x,z) = \frac{\hbar\Delta}{2}\ln(1+s)\,, \tag{1}$$

with $s = \frac{I(x,z)}{I_{\mathrm{sat}}} \times \frac{1}{1+\left(\frac{2\Delta}{\Gamma}\right)^2}$. This potential can be approximated by

$$U_{\mathrm{cw}}(x,z) \simeq \frac{\hbar\Gamma^2}{8\Delta}\frac{I(x,z)}{I_{\mathrm{sat}}} \tag{2}$$

in the limit $s \ll 1$ and $\Delta \gg \Gamma$. Atoms immersed into this field are attracted towards the nodes (antinodes) for blue (red) detuning Δ of the near-resonant laser light. In cesium, the $(F = 4, m_F = 4) \rightarrow (F' = 5, m'_F = 5)$ transition very closely resembles a two-level system with $\Gamma = 1/\tau = 3.3 \times 10^7\ \mathrm{s}^{-1}$ and $I_{\mathrm{sat}} = 1.1\ \mathrm{mW/cm^2}$. In the standard geometry (Fig. 1) the envelope of the light field intensity $I(x,z)$ varies smoothly along the z-propagation direction of the atomic beam, and it is modulated sinusoidally at the half-wavelength scale in the transverse x-direction as

$$I(x,z) = I_{\max}\sin^2(kx)\exp\left(-2\frac{z^2}{w_z^2}\right). \tag{3}$$

The typical length scales in our experiment are $w_z = 84\,\mu$m and $\lambda/2 = \pi/k$ with $\lambda = 852$ nm, and we will neglect the

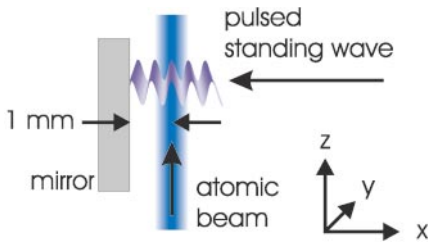

Fig. 1. Schematic setup of our standing wave focusing experiment. The atomic beam propagates in the z direction and traverses the standing wave at a distance of 1 mm from the mirror

slow variation of the laser beam profile in the y direction ($w_y = 788\,\mu\text{m}$).

Theoretically the dipole force exerted by a continuous standing wave light field is a consequence of the steady-state solution to the optical Bloch equations which are applicable as long as the variation of atom–field coupling is slow compared to atomic relaxation. Along the z direction the typical time scale of change at an average thermal velocity $v_{\text{th}} = 300\,\text{m/s}$ is $w_z/v_{\text{th}} \simeq 280\,\text{ns}$, much longer than the cesium spontaneous life time of 30.5 ns.

In a pulsed standing wave derived from a mode-locked laser the situation is very different: the pulse duration is of order $\tau_{\text{p}} = 30$–$80\,\text{ps}$ only. Therefore the atom–field coupling varies extremely rapidly and, in addition, a standing wave exists only in the immediate vicinity of the retroreflecting mirror. However, in our case it still extends over 5–12 mm and is hence sufficiently long to fully cover the atomic beam of cross section 0.1–1 mm (see Sect. 2). Furthermore, at our pulse repetition rate of 80 MHz an atom is on average subject to a train of more than 50 intense pulses when it traverses the pulsed light field. It is thus obvious to investigate the properties of the average force exerted by the pulsed light field.

In our theoretical analysis we will study the dynamical behavior of the Bloch vector which has components (u, v, w) yielding the quadratures of the complex dipole moment $d = (u + \mathrm{i}v)d_{\text{eg}}$. Here we use the rotating wave approximation, d_{eg} designates the dipole matrix element, and w gives the inversion.

During the very short presence of the light field we can completely neglect relaxation and restrict the analysis to the coherent atom–field coupling:

$$\dot{u} = \Delta v\,, \tag{4}$$

$$\dot{v} = -\Delta u - \Omega(x, z, t)w\,, \tag{5}$$

$$\dot{w} = \Omega(x, z, t)v\,, \tag{6}$$

with the Rabi frequency $\Omega = \Gamma(I/2\,I_{\text{sat}})^{1/2}$. (4) can also be written as

$$\dot{\boldsymbol{S}} = \boldsymbol{T} \times \boldsymbol{S}\,, \tag{7}$$

with the Bloch vector $\boldsymbol{S} = (u, v, w)$ which is acted on by the torque $\boldsymbol{T} = (\Omega(x, z, t), 0, -\Delta)$ derived from the laser pulse.

The transverse momentum transfer, or kick due to a single pulse for an atom at position (x, z) is given by

$$\Delta p(x, z) = -\frac{\hbar}{2}\int\limits_{\tilde{\tau}_{\text{p}}} u(x, z, t)\frac{\partial}{\partial x}\Omega(x, z, t)\,\mathrm{d}t\,. \tag{8}$$

Here $\tilde{\tau}_{\text{p}}$ designates an effective pulse length which can formally be extended to $\pm\infty$ with negligible error. In order to allow deterministic focusing of an atomic beam in analogy to the conservative cw potential of (1) the action of a single kick exerted onto an atom must depend on position only. We will now show that this situation is easily obtained if the condition of adiabatic following is fulfilled. In this limit the atomic dipole moment is allowed to adiabatically follow the driving field of the laser pulse. The experimental condition for this situation is

$$\frac{|\dot{\Omega}\Delta|}{\left(\Omega^2 + \Delta^2\right)^{3/2}} \ll 1\,, \tag{9}$$

which can be approximated by

$$|\dot{\Omega}/\Omega| \ll \Delta\,. \tag{10}$$

For our pulsed standing wave $I(x, z, t) = I_0(x, z)\text{sech}^2\left(1.76\frac{t}{\tau_{\text{p}}}\right)$ with $I_0(x, z) = I_{\max}\sin^2(kx)\exp\left(-2\frac{z^2}{w_z^2}\right)$, the time variation of the coupling constant can be evaluated as $|\dot{\Omega}/\Omega| \leq 1.76/\tau_{\text{p}}$ and hence we arrive at a condition for the pulse duration–detuning product,

$$|\tau_{\text{p}}\Delta| \gg 1.76\,. \tag{11}$$

For illustration we show the evolution of the Bloch vector for adiabatic and non-adiabatic conditions and experimentally realistic parameters in Fig. 2.

In Fig. 2a the Bloch vector after the pulse more or less is the same as before, leading to well-defined conditions when the next pulse arrives $T_{\text{p}} = 12.5\,\text{ns}$ later. In the non-adiabatic case the u and v components after the pulse oscillate with a large amplitude (Fig. 2b), which will be radiatively damped by a factor $\exp(-\Gamma T_{\text{p}}/2) = 0.81$ only by the time the next pulse arrives. The momentum transfer (8) due to the next pulse then depends on the history of previous pulse interactions. Our simulations show that in this case the average force exerted onto atoms traversing the standing wave light field shows a non-deterministic behavior and eventually just vanishes. Fulfilling the adiabatic condition thus provides a simple solution to this problem by always returning the atom in its initial state after the interaction with the light field.

1.1 Approximate analytic solution

The adiabatic condition can be interpreted as a narrow and rapid precession of the Bloch vector $\boldsymbol{S}$ around $\boldsymbol{T}$, i. e. $\boldsymbol{S} \parallel \boldsymbol{T}$, and hence in this approximation the u component is simply the normalized projection of $\boldsymbol{T}$ onto the u axis:

$$u(x, z, t) = \frac{\Omega(x, z, t)}{\sqrt{\Omega^2(x, z, t) + \Delta^2}}\,. \tag{12}$$

The average force per pulse cycle then is given by

$$\boldsymbol{F}(x, z) = \frac{\Delta p(x, z)}{T_{\text{p}}} = -\frac{\hbar}{2T_{\text{p}}}\int\limits_{\tilde{\tau}_{\text{p}}} \frac{\Omega(x, z, t)\frac{\partial}{\partial x}\Omega(x, z, t)}{\sqrt{\Omega^2(x, z, t) + \Delta^2}}\,\mathrm{d}t\,, \tag{13}$$

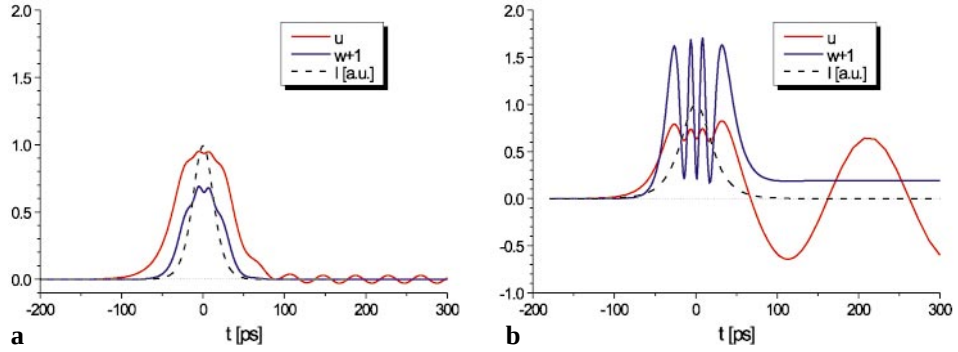

Fig. 2a,b. Numerically simulated evolution of the Bloch vector (u and w components). **a** Adiabatic conditions ($\tau_p = 30$ ps, $\Delta = 2\pi \times 25$ GHz, $\tau_p\Delta = 4.7$) **b** Non-adiabatic conditions ($\tau_p = 30$ ps, $\Delta = 2\pi \times 5$ GHz, $\tau_p\Delta = 0.94$). The *dashed curve* shows the laser intensity I

which can be derived from an effective potential $\boldsymbol{U}_{\rm eff}(x, z)$

$$\boldsymbol{F}(x, z) = -\frac{\partial}{\partial x}\boldsymbol{U}_{\rm eff}(x, z)\,, \tag{14}$$

with

$$\boldsymbol{U}_{\rm eff}(x, z) = \frac{\hbar}{2T_{\rm p}} \int\limits_{\tilde{\tau}_{\rm p}} \left(\sqrt{\Omega^2(x, z, t) + \Delta^2} - \Delta\right) {\rm d}t\,. \tag{15}$$

In Fig. 3 the dependence of the potential from I/Δ for various detunings Δ is shown.

We have checked the validity of this approximation for $\boldsymbol{F}$ by comparing it with the numerical integration of the Bloch equations. Figure 4 shows trajectories calculated with numerical integration and the approximation of (13), for parameters that fulfil the adiabatic condition. The atomic trajectories look nearly the same for both cases, i.e. our approximations are applicable. In fact, for most of our experimental parameters the adiabatic condition is fulfilled even better and the agreement between both simulations is better than in Fig. 4. Not only does this approximation lead to a much more rapid computation of the atomic trajectories, it also provides a transparent solution of the problem.

In the limit $\Omega(x, z, t) \ll \Delta$ which is equivalent to $I_0(x, z) \ll I_{\rm sat} 2(\Delta/\Gamma)^2$ the potential (15) can be expressed as

$$\boldsymbol{U}(x, z) = \frac{\hbar\Gamma^2}{8\Delta}\frac{\bar{I}(x, z)}{I_{\rm sat}}\,, \tag{16}$$

with the average intensity $\bar{I}(x, z) = I_0(x, z)\frac{\tau_p}{0.88T_p}$ for sech^2 pulses. It agrees with the potential $\boldsymbol{U}_{\rm cw}$ (2) for cw laser radiation. Consequently, in this limit for a given average intensity and detuning a pulsed standing wave exerts a dipole force which very nearly equals the cw case.

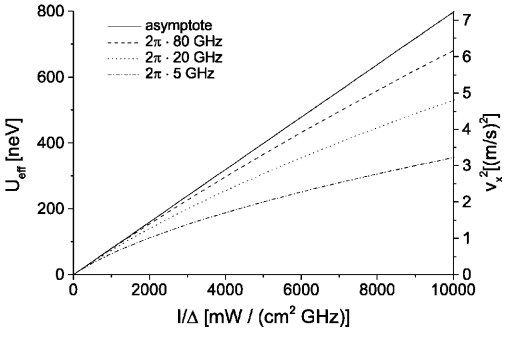

Fig. 3. The potential of the pulsed standing wave for different detunings (pulselength $\tau_p = 80$ ps). To give an idea of the magnitude of the potential the square of the corresponding transverse velocity for cesium atoms is shown on the right axis

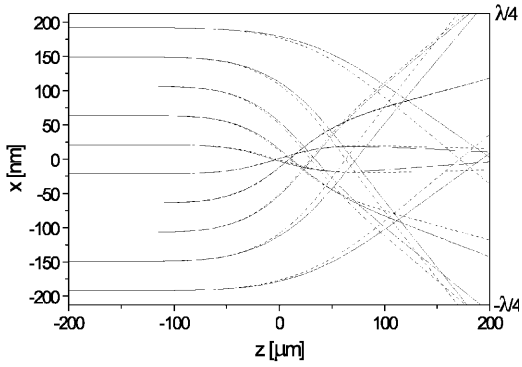

Fig. 4. Simulation of atomic trajectories in one period of the standing wave. *Solid line*: numerical integration of the Bloch equation. *Dashed line*: calculated with the approximated force of (13). Parameters: $v = 300$ m/s, $\tau_p = 80$ ps, $\Delta = 2\pi \times 5$ GHz, $\tau_p\Delta = 2.5$, $P = 100$ mW

These results suggest transferring the concepts of cw atomic beam focusing to the pulsed standing wave case. In the next section we will present experimental evidence that this assumption is valid over a large range of parameters but we will also show some limitations.

2 Experimental

We use a thermal cesium atomic beam which is transversely collimated by laser-cooling methods to a divergence less than 1 mrad (see Fig. 5). The diameter of the atomic beam after the collimation zone is defined by an aperture of diameter 1 mm. A slit of 100 μm width in the x direction can be translated into the atomic beam before the standing-wave interaction zone. The atomic beam profile is analyzed at a distance of 1.24 m beyond the interaction region, where it traverses a resonant laser beam and the fluorescence is monitored with a CCD camera. This apparatus already was used for the production of periodic nanostructures with a cw standing wave and is described in detail in [8]. The pulsed laser beam is sent to the apparatus via a polarization-preserving single-mode optical fiber. We measured pulse shape and pulse length in front of and behind the fiber with an autocorrelator (FR-103, Femtochrome Research, Inc.) and found no change.

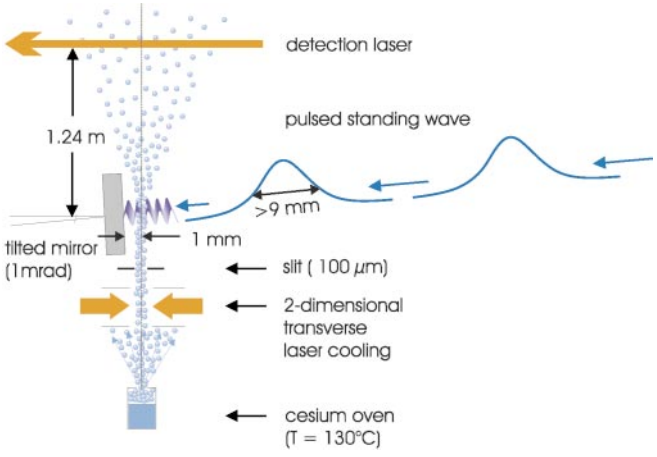

Fig. 5. Schematic experimental setup to measure the beam profile behind the standing wave. The pulse length is varied between 30 and 80 ps and the standing wave extends over 5–12 mm from the mirror. The atomic beam (about 1 mm distance from the mirror) thus is fully covered by the standing wave. The power of the standing wave is varied from 0 to 464 mW, the detuning of the laser from the Cs-D_2 line at 852 nm is set between 5 and 200 GHz

We have used two methods to experimentally investigate the focusing properties of our pulsed standing wave. For the narrow atomic beam (width 0.1 mm) interacting with the standing wave the spatial distribution at large separation (1.24 m) reflects the angular distribution of the atoms leaving the standing wave and makes a rough quantitative analysis of the light forces exerted by the standing wave available. This method gives only indirect indications of the nanoscale focusing properties, but it allows a rapid evaluation of the influence of the experimental parameters pulse length, detuning, and intensity. During these measurements we optically pumped the atoms into the ($F = 4$, $m_F = 4$) groundstate with a weak σ^+ polarized laser beam tuned to the $(F = 4) \rightarrow (F' = 5)$ transition before they entered the σ^+ polarized standing wave.

A direct proof for the periodic focusing of cesium atoms in the pulsed standing wave is given by our second method which provides an image of the spatial distribution of atoms in the focal region through high-resolution lithography with a resist-based technique [11].

2.1 Angular distribution

Because of the nanoscale focusing of the atomic beam in the interaction region the atomic beam expands behind the standing wave. From the resulting transverse density distribution we can derive a measure for the interaction potential in the standing wave by comparing the measured profiles with simulated profiles. We have found that the sensitivity of this method can be increased by tilting the standing wave by a small angle $\beta = 1$ mrad with respect to the atomic beam (Fig. 5): with a perpendicular standing wave the expansion of the atomic beam already saturates at relatively small potentials, whereas the tilted standing wave gives more significant information about higher potential values. In the beam profile behind the tilted standing wave a second peak appears since atomic trajectories are concentrated near the reflecting angle $-\beta$ of the potential wells of the standing wave field (Fig. 6). Note that the Doppler shift introduced by the small angle β is negligible compared to the large detuning of the laser from resonance.

For the comparison of the measured beam profiles with theoretical calculations we simulate a thermal atomic beam with transverse velocity distribution and light field parameters as in our experiment. The trajectories of the atoms traversing the pulsed standing wave are calculated using the expression for the average force (13). Measured and simulated beam profiles (Fig. 7) show a good agreement at a pulse length of $\tau_p = 80$ ps.

Next we have extracted a potential height from a comparison of measured profiles and simulations by calibrating the measured profiles against a set of simulated profiles with different I and Δ. The maximum potential height of the simulated profile, that correlates best with the measured profile, is taken as the maximum potential height of the measurement. In the limit $\Omega(x, z, t) \ll \Delta$ the only variable parameter is I/Δ which simplifies the interpretation of the experimental results.

The result is shown in Fig. 8, lending confidence to the validity of our model for a pulse length of 80 ps and for the investigated parameter range. In contrast, for shorter pulse lengths (30 ps and 50 ps) and large laser power, experimental results render this theoretical approximation invalid: in this case we have obtained large differences between measured and simulated profiles, although the adiabatic condition (11) is well fulfilled for all sets of experimental parameters (Fig. 9).

2.2 Spatial distribution in the focal region

The results of the previous section suggest that the atoms are periodically focused inside the standing wave for a wide range of laser parameters. But a convincing proof has still to be given by a direct measurement of the flux density distribution inside the standing wave.

The theoretically expected force in a blue-detuned pulsed standing wave causes a focusing of the atoms into the min-

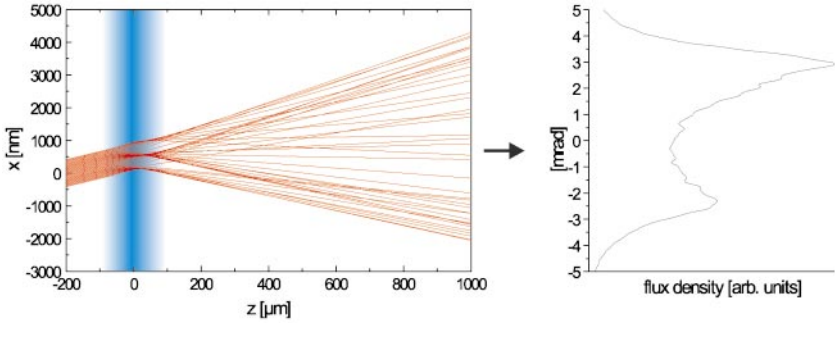

Fig. 6. Simulated atomic trajectories for a standing wave tilted by $\beta = 2.5$ mrad ($P = 400$ mW, $\Delta = 2\pi \times 30$ GHz). The atomic beam in this simulation only illuminates two periods of the standing wave. Some of the atoms are reflected by the potential wells of the standing wave leading to a second peak in the density distribution. On the right-hand side the resulting distribution 1.24 m behind the standing wave is shown. For illustrating purposes we only show trajectories for $v_z = 250$ m/s

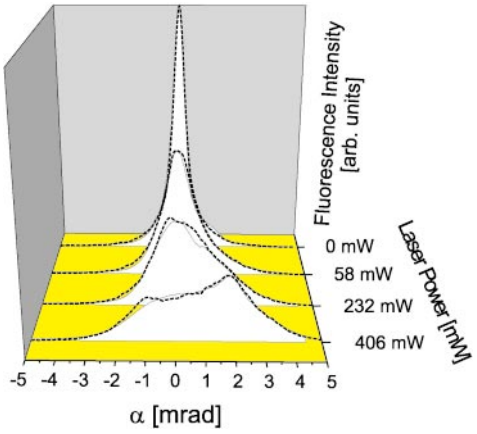

Fig. 7. Comparison of the measured beam profiles (*solid lines*) with simulated profiles (*dashed lines*) 1.24 m behind the interaction zone at $\tau_p = 80$ ps showing good agreement ($\Delta = 2\pi \times 30$ GHz). The beam profiles reflect the angular distribution $f(\alpha)$ of atoms after having traversed the standing wave. Without the standing wave the atomic beam is centered around $\alpha = 0$. Atoms leaving the interaction region perpendicular to the standing wave appear at $\alpha = 1$ mrad

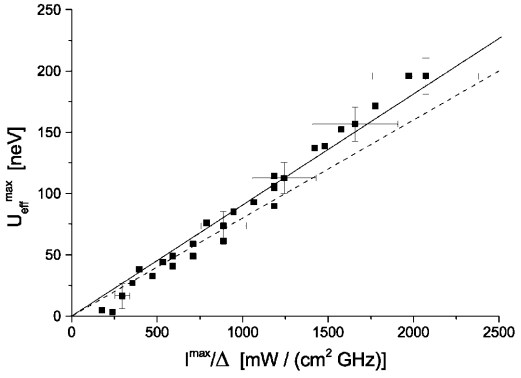

Fig. 8. Maximum potential heights derived from a comparison of experimental and simulated beam profiles. The *solid line* is a linear fit through the origin to experimentally determined potential values where the condition $\Omega \ll \Delta$ is fulfilled. The slope of this curve is 12% larger than the theoretically expected one (*dashed line*). This deviation lies within the systematic experimental uncertainty ($\approx 15\%$) of determining I/Δ. The error bars in y direction indicate statistical errors of the simulated beam profiles

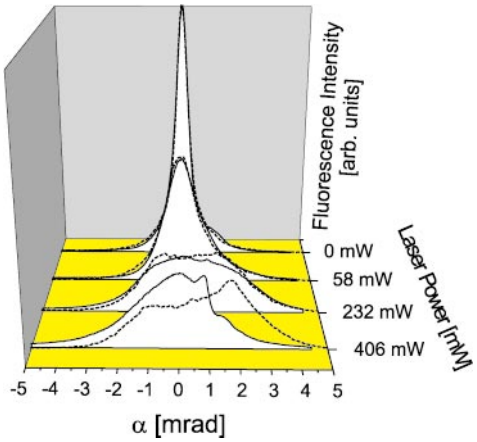

Fig. 9. Comparison of the measured beam profiles (*solid lines*) with simulated profiles (*dashed lines*) 1.24 m behind the interaction zone at $\tau_p = 50$ ps ($\Delta = 2\pi \times 30$ GHz). For large laser power (406 mW) a strong deviation of experiment and simplified theory is observed.

ima of the standing wave. This leads to a characteristic flux density distribution inside the interaction region, i.e. the flux density increases in regions of small light intensity and decreases in regions of high intensity (Fig. 10). The variation of the cesium flux density inside the standing wave can be investigated with a lithographic method based on a high-resolution resist. We use a self-assembling monolayer (SAM) of nonanthiole on gold [11].

The schematic experimental setup for these investigations is shown in Fig. 11. In this case, unlike the experiments in the previous section we use the full 1-mm-diameter atomic beam and a standing wave aligned perpendicular to the atomic beam to achieve maximum contrast. Furthermore, we employed a different optical pumping scheme [12] to avoid transverse heating of the atomic beam. The parameters we have chosen for the experiments were $P = 350$ mW, $\Delta = 2\pi \times 20$ GHz, and $\tau_p = 80$ ps.

The result of the lithographical experiment is shown in Fig. 12. As expected, the substrate is patterned with a regular line structure of periodicity $\lambda/2 = 426$ nm, clearly demonstrating the microscopic periodic focusing ability of a pulsed standing wave. The resist-based lithography process introduces small irregularities which we have also found in experiments with a continuous, single-frequency standing wave.

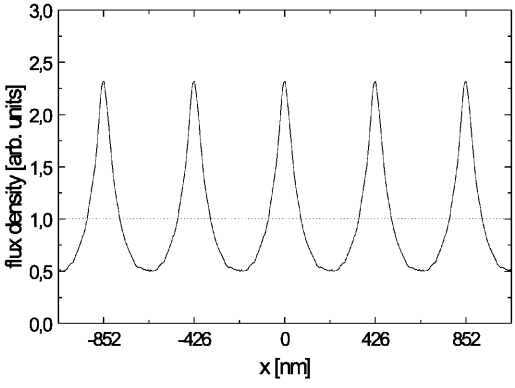

Fig. 10. Simulated flux density distribution of the atomic beam in the focal plane shown over 5 periods of the pulsed standing wave. Parameters: $P = 100$ mW, $\Delta = 2\pi \times 30$ GHz, $\tau_p = 60$ ps. The *dotted line* indicates the flux density without standing wave

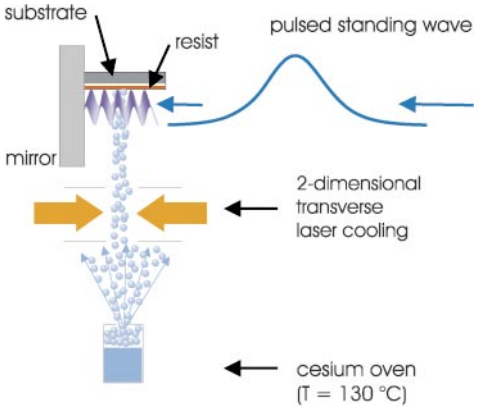

Fig. 11. Experimental setup for high-resolution lithography with a pulsed standing wave. The resist-coated substrate is placed inside the standing wave light field

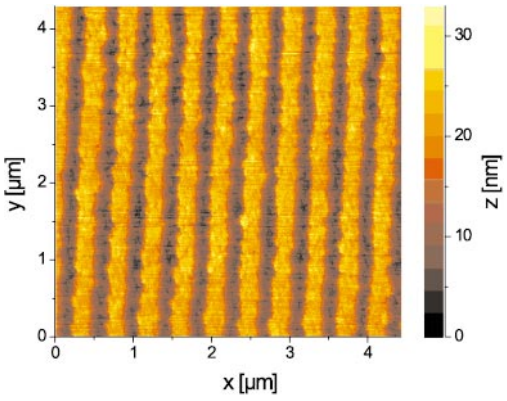

Fig. 12. Atomic force microscope picture of an exposed and developed substrate. The regular lines with a periodicity of $\lambda/2 = 426\,\mathrm{nm}$ result from the spatially flux density distribution of the cesium atomic beam caused by the pulsed standing wave. Parameters: $P = 350\,\mathrm{mW}$, $\Delta = 2\pi \times 20\,\mathrm{GHz}$, $\tau_\mathrm{p} = 80\,\mathrm{ps}$

3 Conclusion

We have theoretically and experimentally investigated the periodic focusing of a cesium atomic beam in a pulsed standing wave. Theoretically we expect that an atomic beam is periodically focused in a near-resonant standing wave, as long as the adiabatic condition $|\tau_\mathrm{p}\Delta| \gg 1.76$ is fulfilled. In the limit $\Omega \ll \Delta$ the force on the atoms is nearly the same as in the cw case for $s \ll 1$ and $\Delta \gg \Gamma$.

To determine the force quantitatively we have measured the spatial expansion of the atomic beam in the far field of the standing wave. From these measurements we have extracted information about the focusing in the interaction region by comparing measured beam profiles with simulated profiles. This method allows a rapid evaluation of experimental parameters. For long pulses (80 ps) we have found a good agreement of our theory and the experimental results for all investigated experimental parameters.

For shorter pulses ($\leq 50\,\mathrm{ps}$) and high values of I/Δ we have found a significant difference between our simplified theory and the experimental investigations even though the adiabatic condition is still fulfilled.

Experimentally we have proven with nanoscale lithographic experiments, that the spatial atomic flux density distribution inside the standing wave is modulated with periodicity $\lambda/2$ due to the focusing of the atomic beam into the minima of the blue-detuned standing wave light field. Thus it should be possible to extend atom lithography to technologically interesting elements with blue or ultraviolet resonance lines by using frequency-doubled pulsed lasers.

Acknowledgements. We would like to thank M. Zehnpfennig for his assistance in the early stage of the experiment, as well as H. Merimeche and R. Bertram for experimental support. We are very much indebted to H. Metcalf for discussions, ideas, and his unlimited enthusiasm. This work was partially funded by the EC within the TMR network Nanofab, contract ERBFMRXCT-0129.

References

1. G. Timp, R.E. Behringer, D.M. Tennant, J.E. Cunningham, M. Prentiss, K.K. Berggren: Phys. Rev. Lett. **69**, 1636 (1992)
2. W. R. Anderson, C.C. Bradley, J.J. McClelland, R.J. Celotta: Phys. Rev. A **59**, 2476 (1999)
3. J.J. McClelland, R.E. Scholten, E.C. Palm, R.J. Celotta: Science **262**, 877 (1993)
4. U. Drodofsky, J. Stuhler, B. Brezger, T. Schulze, M. Drewsen, T. Pfau, J. Mlynek: Microelectron. Eng. **35**, 285 (1997)
5. R. Gupta, J.J. McClelland, Z.J. Jabbour, R.J. Celotta: Appl. Phys. Lett. **67**, 1378 (1995)
6. U. Drodofsky, J. Stuhler, T. Schulze, M. Drewsen, B. Brezger, T. Pfau, J. Mlynek: Appl. Phys. B **65**, 755 (1997)
7. R.W. McGowan, D.M. Giltner, S.A. Lee: Opt. Lett. **20**, 2535 (1995)
8. F. Lison, H.-J. Adams, D. Haubrich, M. Kreis, S. Nowak, D. Meschede: Appl. Phys. B **65**, 419 (1997)
9. A. Goepfert, I. Bloch, D. Haubrich, F. Lison, R. Schütze, R. Wynands, D. Meschede: Phys. Rev. A **56**, R3354 (1997)
10. J. Dalibard, C. Cohen-Tannoudji: J. Opt. Soc. Am. B **2**, 1707 (1985)
11. M. Kreis, F. Lison, D. Haubrich, D. Meschede, S. Nowak, T. Pfau, J. Mlynek: Appl. Phys. B **63**, 649 (1996)
12. A. Avila, V. Giordano, V. Candelier, E.D. Clercq, G. Theobald, P. Cerez: Phys. Rev. A **36**, 3719 (1987)